ORIGINAL ARTICLE

Quantitative In Vivo Magnetic Resonance Imaging of Multiple Sclerosis at 7 Tesla with Sensitivity to Iron

Kathryn E. Hammond, BS,[1,2] Meredith Metcalf, BS,[1,2] Lucas Carvajal, PhD,[2] Darin T. Okuda, MD,[3] Radhika Srinivasan, PhD,[2] Dan Vigneron, PhD,[2] Sarah J. Nelson, PhD,[2,4] and Daniel Pelletier, MD[3]

Objective: Magnetic resonance imaging at 7 Tesla produces high-resolution gradient-echo phase images of patients with multiple sclerosis (MS) that quantify the local field shifts from iron in the basal ganglia and lesions. Phase imaging is easily integrated into clinical examinations because it is a postprocessing technique and does not require additional scanning. The purpose of this study was to quantify local field shifts in MS and to investigate their relation to disease duration and disability status.

Methods: Thirty-two subjects including 19 patients with MS and 13 age- and sex-matched control subjects were scanned at a spatial resolution of up to 195 $\times$ 260μm. Data were postprocessed to produce anatomical quantitative phase images of local field shifts, as well as conventional magnitude images.

Results: The phase images showed an increased local field in the caudate, putamen, and globus pallidus of patients relative to control subjects ($p < 0.01$). The local field in the caudate was strongly correlated with disease duration ($r^2 = 0.77$; $p < 0.001$). Phase images showed contrast in 74% of the 403 lesions, increasing the total lesion count by more than 30% and showing distinct peripheral rings and a close association with vasculature.

Interpretation: The increased field in the basal ganglia and correlation with disease duration suggest pathological iron content increases in MS. The peripheral phase rings are consistent with histological data demonstrating iron-rich macrophages at the periphery of a subset of lesions. The clearly defined vessels penetrating MS lesions should increase our ability to detect focal vascular abnormalities specifically related to demyelinating processes.

Ann Neurol 2008;64:707–713

Ex vivo postmortem histological stains of the brain have shown that iron accumulates in neurodegenerative diseases such as Alzheimer's,[1,2] Huntington's,[3,4] and Parkinson's[3] diseases. Previous studies in MS have identified iron accumulation in both the deep gray matter (basal ganglia)[5] and plaques,[2,6] but because they were performed ex vivo, they did not establish whether iron was primary to and caused MS pathology or whether iron accumulation was secondary to chronic inflammation in MS. An in vivo contrast mechanism sensitive and specific to the presence of iron may contribute substantially to understanding the role of iron in neurodegenerative pathology and developing iron-based biomarkers for disease progression.

The high signal-to-noise ratio (SNR) of 7 Tesla magnetic resonance imaging (MRI) allows for in vivo visualization of anatomical structures at submillimeter resolutions only previously attainable ex vivo. We recently developed a new 7 Tesla technique[7] that enabled high-resolution quantitative imaging of the local field shift (LFS) caused by magnetic susceptibility-shifted compounds such as iron. The technique postprocesses the phase of a gradient-recalled echo scan to measure the LFS. Because iron is paramagnetic,[8] its presence increases the local magnetic field (a positive LFS) and accelerates the ^{1}H precession, causing phase to accumulate over the echo time (TE).

Previous in vivo attempts to monitor iron in the basal ganglia in neurodegenerative diseases using T2[5,9,10] or magnetic field correlation[11] yielded inconsistent findings,[3,12] potentially because of confounding changes in diffusion[13] that affect these contrast mechanisms. It would be even more difficult to use these contrast mechanisms to interrogate iron in MS lesions because they would be heavily confounded by the changes in both relaxation and diffusion. Phase imag-

From the [1]University of California San Francisco/Berkeley Joint Graduate Group in Bioengineering; [2]Department of Radiology, Surbeck Laboratory for Advanced Imaging, University of California San Francisco; [3]Department of Neurology, University of California, San Francisco; and [4]Program in Bioengineering, University of California San Francisco, San Francisco, CA.

Received May 23, 2008, and in revised form Sep 9. Accepted for publication Oct 17, 2008.

Potential conflict of interest: Nothing to report.

Published online Mon 00, 2008, in Wiley InterScience (www.interscience.wiley.com). DOI: 10.1002/ana.21582

Address correspondence to Dr Pelletier, UCSF Multiple Sclerosis Center, 350 Parnassus Avenue, Suite 908, San Francisco, CA 94117. E-mail: daniel.pelletier@ucsf.edu

ing at 7 Tesla offered the specificity to LFS, the insensitivity to relaxation and diffusion, and the high spatial resolution to assess for the presence of iron in both the basal ganglia and MS lesions.

Iron accumulation in neurodegenerative diseases[1–6,14] results from a cyclic inflammatory process. Inflammation increases local iron content by attracting iron-rich macrophages,[2,6] disrupting the blood–brain barrier[6] and reducing axonal clearance of iron.[14–17] Iron can be safely stored in the brain as ferritin, a water-soluble storage protein that sequesters iron, but when iron overload or disruptions in cellular iron management cause some iron to be stored as hemosiderin or free iron, it has the potential to exchange electrons with surrounding molecules.[14] Numerous studies of iron in MS and experimental allergic encephalomyelitis (an animal model of MS) have shown that free iron or iron overload forms highly reactive hydroxyl radicals.[18–21] These free radicals initiate lipid peroxidation leading to cell membrane dysfunction[22] and chronic microglial activation.[17] Inhibition of enzymes in the respiratory chain induces mitochondrial dysfunction, which reduces cellular energy production because of hypometabolism[23,24] and causes hypoxia that drives progressive axonal dysfunction.[15–17] The presence of iron-rich cells and the inability to clear iron eventually cause further inflammation and iron deposition, initiating a cyclic process evidenced by the accumulation of iron in neurons and oligodendrocytes,[6] the basal ganglia,[5] and macrophages and microglia[2,6] seen in postmortem MS brains.

The purpose of this study was to evaluate whether the presence of iron in the basal ganglia and MS lesions could be observed and quantified in vivo using 7 Tesla phase imaging.

Subjects and Methods

Data Acquisition

Thirty-two subjects including 19 relapsing-remitting MS patients (7 untreated; 4 on glatiramer acetate for a mean time of 3.2 years; 4 on interferon-β therapy for a mean time of 7.2 years; 4 on natalizumab for a mean time of 0.5 year) and 13 age- and sex-matched control subjects (Table 1) were scanned on a whole-body GE EXCITE 7T (General Electric Healthcare Technologies, Waukesha, WI) equipped with an 8-channel receive phased array coil (commercially available from NOVA Medical, Wilmington, MA, or built in-house by L.C.) and a head transmitter coil with active detuning. Axial gradient-recalled echo images were acquired at a spatial resolution of 195 × 260μm or 350 × 350μm: echo/repetition time (TE/TR) of 12 to 15/250 milliseconds, 20-degree flip angle, 2mm slice thickness, matrix/field of view 1,024 × 768/20cm or 512 × 512/18cm, 3 repetitions (number of excitations), and scan time 9 or 6.5 minutes. No contrast (ie, gadolinium) was administered. The image volume was obliqued to contain the anterior and posterior commissures.

Data Processing and Image Analysis

The magnitude and phase images were created as Hammond and colleagues[7] described. As shown in Figure 1, regions of interest (ROIs) in the basal ganglia were manually drawn around the caudate, putamen, thalamus, and globus pallidus. Additional ROIs were placed around the white matter regions of the splenium of the corpus callosum and the posterior internal capsule. ROIs were placed on both the left and right sides in each slice containing the structure. The final value for each structure in each subject was calculated by averaging the mean pixel value of each ROI.

Phase images (measured in radians) were converted to LFS maps (measured in parts per billion [ppb]) by subtracting the mean phase of the posterior internal capsule, dividing by ($2\pi \times$ TE) to measure the local frequency of ^{1}H precession

Table 1. **Characteristics of Patient and Control Populations**

Subject Demographics	Patients	Control Subjects	*p*
n	19	13	—
Sex, M/F	6/13	5/8	—
Mean age ± SD, yr	42.32 ± 12.90	40.15 ± 14.19	0.65
Mean disease duration ± SD, yr	12.0 ± 7.6	—	—
Mean EDSS score ± SD	2.1 ± 1.2	—	—
Mean LFS ± SD, ppb			
Globus pallidus (ppb)	20.33 ± 4.19(n=12)	15.94 ± 2.68(n=11)	<0.005
Caudate (ppb)	20.06 ± 5.10(n=14)	16.14 ± 3.59(n=12)	<0.01
Putamen (ppb)	14.33 ± 3.96(n=15)	9.66 ± 2.15(n=12)	<0.0001
Thalamus (ppb)	9.56 ± 3.02(n=14)	8.09 ± 2.08(n=12)	0.06
Corpus callosum (ppb)	4.40 ± 2.45(n=15)	4.46 ± 1.71(n= 9)	0.47

SD = standard deviation; EDSS = Expanded Disability Status Scale; LFS = local field shift; ppb = parts per billion.

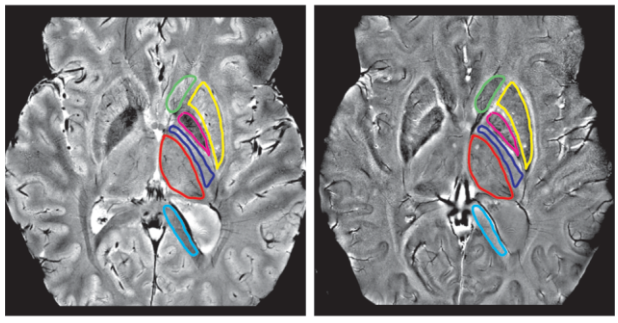

Fig 1. Regions of interest (ROIs) were drawn on the high-resolution 7-Tesla gradient-recalled echo (GRE) magnitude (left) and phase (right) images: head of caudate (green), putamen (yellow), globus pallidus (pink), thalamus (red), posterior internal capsule (blue), and splenium of the corpus callosum (cyan).

(measured in Hertz), and dividing by ($\gamma \times B_0$) to normalize the MRI magnet strength (B_0). Converting phase images to LFS maps enabled making comparable measurements across the two scan parameters that affect phase contrast: MRI field strength (eg, 1.5, 3, or 7 Tesla) and TE. In units of parts per billion, LFS caused by iron was expected to be independent of the field strength or TE because magnetic susceptibility scales linearly with field strength[8] and phase scales linearly with TE.[7] Three MS patients and one control subject were excluded from the analysis of the basal ganglia because the field of view was placed superior to the basal ganglia. The mean LFS in MS patients were compared with healthy control subjects using Student's *t* test. The correlations between LFS and MS disease duration, Expanded Disability Status Scale (EDSS) score, or subject age were calculated using the Pearson product moment correlation coefficient.

MS lesions were counted and classified according to whether they were visible only in the magnitude image, visible only in the phase image, or visible in both the magnitude and phase images. Lesions were further classified according to whether they contained penetrating veins and peripheral rings.

Results

Basal Ganglia

Characteristics of the MS patients and control subjects are presented in Table 1. The LFS was significantly greater in the caudate, putamen, and globus pallidus of MS patients relative to control subjects ($p < 0.01$), and showed a strong trend toward significant increase in the thalamus ($p = 0.06$). The LFS was shifted an additional 4.39ppb (1.31Hz) in the globus pallidus, 3.92ppb (1.17Hz) in the caudate, 4.67ppb (1.39Hz) in the putamen, and 1.47ppb (0.44Hz) in the thalamus. The LFS in the caudate remained significant when the two elevated outliers were removed (Fig 2A). The LFS was not increased relative to control subjects in the splenium of the corpus callosum.

LFS was strongly correlated with MS disease duration in the caudate ($r^2 = 0.77$, $p < 0.001$; see Fig 2B) and moderately correlated in the putamen ($r^2 = 0.39$, $p < 0.05$; see Fig 2C). To eliminate the possibility that the outlier patient with a disease duration of 37 years dominated the correlation (see Figs 2B, C), we removed the subject and found the correlation remained significant in the caudate ($r^2 = 0.53$, $p < 0.05$) but was no longer significant in the putamen ($r^2 = 0.18$). There were no correlations between LFS and age in control subjects in either the caudate ($r^2 = 0.10$; see Fig 2E) or putamen ($r^2 = 0.06$), indicating that the correlations with MS disease duration were not due solely to aging of the patients. There were no correlations between LFS and MS disease duration in other structures (eg, corpus callosum shown in Fig 2D) or between LFS and EDSS in any structures.

Color maps showing increased LFS in the basal ganglia of an MS patient relative to an age- and sex-matched control are shown in Figure 3. The patient was a 41-year-old woman with an 11-year disease duration and an EDSS score of 1.0. The control subject was a 42-year-old woman with no significant medical history. The dark blue color of the MS patient's basal ganglia showed an increased LSF. The LFS maps also differentiated between a positive LFS (an increased

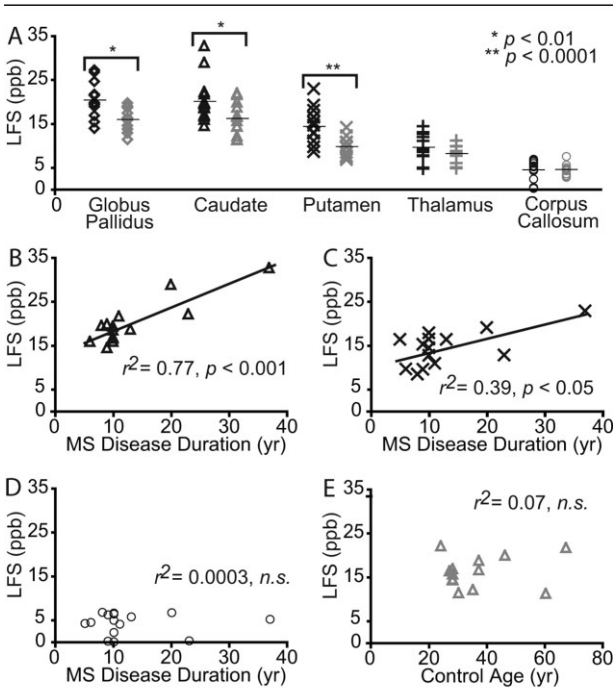

Fig 2. Local field shift (LFS) was significantly increased in the globus pallidus, caudate, and putamen relative to age- and sex-matched control subjects (A). LFS was correlated with disease duration in the caudate (B) and putamen (C), though not in other regions of interest (eg, corpus callosum shown in D). LFS was not correlated with age in healthy control subjects (eg, caudate shown in E). MS = multiple sclerosis; n.s. = not significant. *p < *0.01;* **p < *0.0001.*

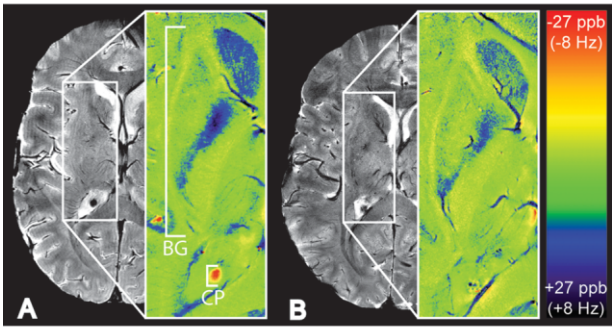

Fig 3. Magnitude (grayscale) and local field shift (LFS; color inset) images of a multiple sclerosis (MS) patient (A) and age- and sex-matched control (B). The cool spectrum of the basal ganglia (BG) *in the MS patient showed an increased field, indicating the local presence of paramagnetic compounds such as iron. The hot spectrum of the calcified choroid plexus* (CP) *showed a decreased field, indicating the local presence of diamagnetic compounds such as calcium.*

magnetic field) and a negative LFS (a decreased magnetic field), as shown in the blue of the basal ganglia and red of the calcified choroid plexus (see Fig 3A). Note that the increased LFS in the basal ganglia was not seen in the magnitude images, and that the magnitude images did not distinguish between increased and decreased magnetic field shifts because both shifts caused signal dropout.

Multiple Sclerosis Lesions

A total of 403 lesions were counted in the 18 MS patients. The phase images showed peripheral phase rings, additional lesions not seen in the magnitude images, and well-defined vessels penetrating lesions. Detecting these additional lesions and unique contrast patterns did not require an additional scan because phase images were created by reprocessing the complex image volume traditionally used to produce magnitude images. The distribution and representative images of lesions by classification are shown in Table 2 and Figure 4.

Phase images identified contrast patterns and additional lesions not seen in the magnitude images. Thirty-one lesions (8% of lesions) had peripheral rings in the phase images (eg, lesions A1 and B1 in Fig 4). The magnitude images did not show whether there was a peripheral field shift; for example, lesions A1 and C1 were virtually identical in the magnitude images, yet there was a strong field shift at the periphery of A1 and almost no phase shift at the periphery of C1.

Phase images identified 89 additional lesions (eg, lesion C2), increasing the total lesion count by almost 30%. Of note, 104 lesions seen in the magnitude images were not seen in the phase images (eg, lesion D1). The remaining 210 lesions, about half of the total 403 lesions, showed both magnitude and phase contrast.

The high spatial resolution and susceptibility-weighting of the phase images provided excellent imaging of veins penetrating MS lesions. The veins appeared narrow and showed high contrast in the phase images. There was a close association between the lesions and the veins: 67% of lesions showed penetrating veins, of which 83% had surrounding field shifts that were quantifiable in the phase images. For example, lesion D2 was shifted about 10ppb relative to the surrounding white matter, whereas lesion D1 was shifted less than 0.1ppb.

Discussion

The in vivo high-resolution 7 Tesla MRI phase images enabled quantitative assessment of the LFS in the deep gray nuclei (see Table 1 and Figs 2 and 3) and showed contrast in lesions consistent with previous ex vivo histological studies (see Fig 4). Phase imaging offered a significant improvement to previous MRI tools available for interrogating iron, providing quantitative LFS maps specific to field shifts and without requiring additional scanning. The high spatial resolution made possible by scanning at 7 Tesla enabled us to interrogate the LFS both in lesions and in the deep gray matter.

Phase Images Showed Increased Local Field Shift in the Basal Ganglia of Multiple Sclerosis Patients

The increased LFS in the basal ganglia and correlation with MS disease duration suggested iron accumulation was associated with MS. Our findings support the contention that local magnetic field shifts cause the T2-hypointensity[5,9,10] and increased magnetic field correlation[25] previously reported in MS patients. The drawback of these previous techniques is that they are sensitive to a wide spectrum of pathology and can be used only with the assumption that there are no other structural changes. Changes in diffusion[13] could explain contradictory findings such as one study that did not observe increased T2-hypointensity in MS patients[12] and another that compared T2 values with tissue assays for iron and showed Huntington's disease patients who had threefold increase in iron but the longest T2.[3] The presence of calcium could also confound the detection of iron. For example, calcium in the basal ganglia of a patient with system lupus erythematosus[26] could be misinterpreted as iron because both calcium and iron cause signal dropout in the magnitude image. In the phase image, calcium could be distinguished from iron because calcium is diamagnetic and decreases LFS, whereas iron is paramagnetic and increases LFS. Diamagnetic and paramagnetic field effects were shown in Figure 3; the calcified choroid plexus was in the red LSF spectrum, whereas the basal ganglia were in the blue LFS spectrum. Note that both

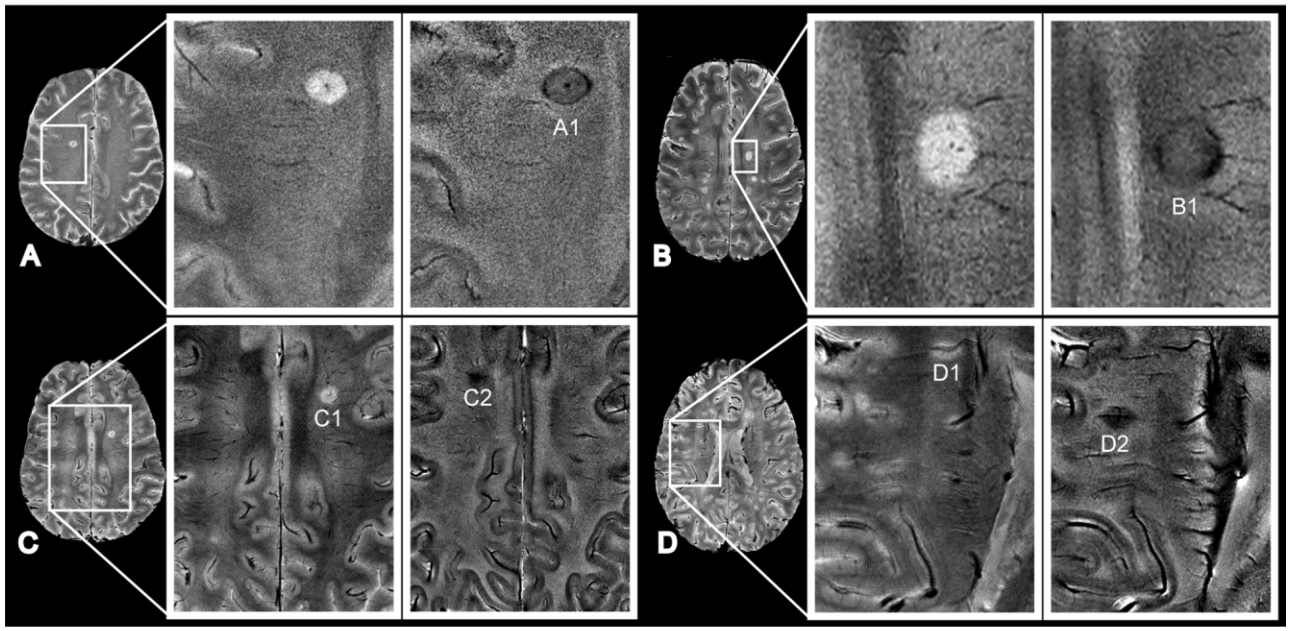

Fig 4. Representative magnitude (left inset) and phase (right inset) images of multiple sclerosis lesions of four patients (A–D). Phase images showed peripheral rings (lesions A1 and B1) and additional lesions (lesion C2) not seen in the magnitude images and well-defined vessels penetrating lesions (lesions A1 and D2). Some lesions were seen only in the magnitude images (lesions C1 and D1).

the choroid plexus and basal ganglia appeared hypointense in the magnitude image.

The finding that LFS was increased relative to control subjects in ROIs in the basal ganglia but not in the splenium of the corpus callosum was consistent with postmortem histological stains showing increased iron in the basal ganglia but not in the white matter.[5] The globus pallidus was slightly less shifted than expected for the reported iron density. It is possible that the low signal-to-noise ratio in the globus pallidus (pink ROI in Fig 1) introduced high noise in the phase image that caused underestimation of the LFS. It was also difficult to estimate the field shift in the thalamus because of the large intrathalamic phase variation. For example, the pulvinar nucleus was hypointense, whereas the mamillothalamic tracts were hyperintense (see Fig 1B). We expect that with more patients and subsegmentation of thalamic ROIs we would find a significant increase in the LFS increase in MS patients as reported for magnetic field correlation.[11]

A limitation of this study was that it did not include cognitive assessments, and thus could not establish correlations with LFS. Future longitudinal studies in a larger population of patients should evaluate iron as a predictor of basal ganglia atrophy,[27] EDSS progression, and neuropsychological test performance to establish whether iron is primary to and causes MS pathology, or whether iron is secondary to MS pathology and simply results from years or decades of inflammatory and neurodegenerative insults.

Lesions Showed Peripheral Phase Rings Consistent with Histology

The spatial patterns of phase contrast we observed in MS lesions were consistent with previous histological studies. Our observation of field shifts at the periphery of 31 lesions (see Table 2 and Fig 4) supported existing histological data identifying iron[28] and a rim of activated microphages[17] at the edge of a subset of lesions. Diaminobenzidine tetrahydrochloride–enhanced Perl's stains have shown the macrophages at the periphery of MS lesions to be rich in iron,[2] presumably from either destruction of oligodendrocytes and myelin, both of which contain iron,[29] or from the extravasation of blood into the brain.[6] It may be possible to use the phase images to differentiate between acute lesions, which are rich in macrophages,[30] and slowly expanding chronic lesions, which are reported to have few macro-

Table 2. **Classification of lesions seen at 7 Tesla**

Lesion Category	Lesion seen in:		
	Magnitude Only	Phase Only	Magnitude and Phase
All (N = 403)	26%	22%	52%
Penetrating vein(s) (N = 268)	17%	27%	56%
Peripheral contrast (N = 31)	0%	94%	6%

phages concentrated at the lesion rim,[17,31] although the presence of globular structures of nonheme iron reported in chronic lesions[32] could confound the differentiation.

The peripheral rings were observed in vivo and without the use of contrast agents. Rings were observed in 8% of lesions, less than the 21% of lesions reported to show edge activity on hematoxylin and eosin staining,[33] but more than the less than 1% observed in the magnitude images. The large slice thickness and low concentration of iron are likely responsible for some of the missed edge activity. If future histological studies confirm that LFS maps give direct detection of iron-rich macrophages, phase imaging could become established as a more sensitive technique for imaging acute inflammation than injecting gadolinium, which detects only blood–brain barrier breakdown,[34,35] and as a less invasive technique than introducing macrophages labeled with ultrasmall particles of iron oxides.[36,37]

Phase Images Showed Quantifiable Field Shifts in Multiple Sclerosis Lesions

We observed phase contrast in 74% of lesions. About 30% of these lesions were not visible in magnitude images, perhaps because magnitude is sensitive to many intrinsic (T1, proton density, diffusion, and so forth) and extrinsic (TR, flip angle, and so forth) parameters that can mask the T2 decrease from iron. For example, T2 lengthening caused by edema, inflammation, and demyelination could mask the decrease in T2 from iron-rich macrophages and cause the magnitude image to appear hyperintense instead of hypointense. In the phase image, the paramagnetic field effects of the iron could be quantified because phase is sensitive only to field shifts. Susceptibility-weighted images,[38] a technique that multiplies a filtered and masked phase image into the magnitude image to enhance contrast in susceptibility-shifted features such as veins, suffers a similar challenge to magnitude images for quantification of iron because of the contrast contribution from the magnitude images.

Phase Images Showed Close Association of Vessels with Lesions

We observed penetrating vessels in 268 of the 403 lesions, supporting the contention that MS progresses along the vasculature[39,40] and affirming the improved detection of microvasculature in MS lesions recently reported at 7 Tesla.[41,42] The 7-Tesla field strength has both high signal-to-noise ratio and high magnetic susceptibility effects, producing high-resolution images sensitive to even very small veins. Phase images had narrower venous definition than magnitude images or expected for susceptibility-weighted images. More than 80% of lesions with penetrating veins had peripheral phase contrast, which may indicate perivenular inflammation and support autopsy findings that inflammation starts around the veins with macrophages emigrating from the veins to digest myelin in response to activation signals.[43]

A limitation of this study was that it did not include measurements of vessel leakiness such as gadolinium enhancement or cerebral perfusion. Future studies comparing longitudinal gadolinium enhancement with lesion LFS may elucidate whether local iron accumulation predicts or follows blood–brain barrier compromise. We do not believe that the perivascular phase contrast is the result of increased leakage caused by increased perfusion since previous studies have reported decreased perfusion in both MS lesions and MS normal-appearing white matter relative to controls.[44] It would be interesting, however, to compare phase with the relative perfusion of acute lesions, which were reported to have greater perfusion than nonacute lesions.

In summary, phase images at 7 Tesla showed novel contrast in high-resolution images of MS lesions and enabled quantitative assessment of the LFS in the deep gray nuclei. The technique was easily integrated into a clinical examination because it used the same scan acquired for conventional magnitude images and, therefore, did not require an additional scan. Increased phase in the basal ganglia supported postmortem histological studies showing excess iron in the basal ganglia. Phase contrast in lesions was consistent with histological studies reporting iron-rich macrophages at the lesion periphery and a close association of lesions with venular vasculature. This quantitative technique showed promise for monitoring disease severity and furthering understanding of MS inflammatory-demyelinating processes in vivo using MRI.

This research was supported by an academic research partnership grant from the University of California in conjunction with GE Healthcare (ITL-BIO04-10148, S.N.), the National Science Foundation Graduate Research Fellowship Program (K.H.), and the United States National Multiple Sclerosis Society (Harry Weaver Neuroscience Scholarship, JF-2122A, D.P.).

References

1. Hallgren B, Sourander P. The non-haemin iron in the cerebral cortex in Alzheimer's disease. J Neurochem 1960;5:307–310.
2. LeVine SM. Iron deposits in multiple sclerosis and Alzheimer's disease brains. Brain Res 1997;760:298–303.
3. Chen JC, Hardy PA, Kucharczyk W, et al. MR of human postmortem brain tissue: correlative study between T2 and assays of iron and ferritin in Parkinson and Huntington disease. AJNR Am J Neuroradiol 1993;14:275–281.
4. Dexter DT, Carayon A, Javoy-Agid F, et al. Alterations in the levels of iron, ferritin and other trace metals in Parkinson's disease and other neurodegenerative diseases affecting the basal ganglia. Brain 1991;114(pt 4):1953–1975.
5. Drayer B, Burger P, Hurwitz B, et al. Reduced signal intensity on MR images of thalamus and putamen in multiple sclerosis: increased iron content? AJR Am J Roentgenol 1987;149:357–363.

6. Craelius W, Migdal MW, Luessenhop CP, et al. Iron deposits surrounding multiple sclerosis plaques. Arch Pathol Lab Med 1982;106:397–399.
7. Hammond KE, Lupo JM, Xu D, et al. Development of a robust method for generating 7.0 T multichannel phase images of the brain with application to normal volunteers and patients with neurological diseases. Neuroimage 2008;39:1682–1692.
8. Schenck JF. The role of magnetic susceptibility in magnetic resonance imaging: MRI magnetic compatibility of the first and second kinds. Med Phys 1996;23:815–850.
9. Bakshi R, Shaikh ZA, Janardhan V. MRI T2 shortening ('black T2') in multiple sclerosis: frequency, location, and clinical correlation. Neuroreport 2000;11:15–21.
10. Russo C, Smoker WR, Kubal W. Cortical and subcortical T2 shortening in multiple sclerosis. AJNR Am J Neuroradiol 1997; 18:124–126.
11. Ge Y, Jensen JH, Lu H, et al. Quantitative assessment of iron accumulation in the deep gray matter of multiple sclerosis by magnetic field correlation imaging. AJNR Am J Neuroradiol 2007;28:1639–1644.
12. Grimaud J, Millar J, Thorpe JW, et al. Signal intensity on MRI of basal ganglia in multiple sclerosis. J Neurol Neurosurg Psychiatry 1995;59:306–308.
13. Filippi M, Bozzali M, Comi G. Magnetization transfer and diffusion tensor MR imaging of basal ganglia from patients with multiple sclerosis. J Neurol Sci 2001;183:69–72.
14. Stankiewicz J, Panter SS, Neema M, et al. Iron in chronic brain disorders: imaging and neurotherapeutic implications. Neurotherapeutics 2007;4:371–386.
15. Bolanos JP, Almeida A, Stewart V, et al. Nitric oxide-mediated mitochondrial damage in the brain: mechanisms and implications for neurodegenerative diseases. J Neurochem 1997;68: 2227–2240.
16. Lucchinetti C, Bruck W, Parisi J, et al. Heterogeneity of multiple sclerosis lesions: implications for the pathogenesis of demyelination. Ann Neurol 2000;47:707–717.
17. Lassmann H, Brück W, Lucchinetti CF. The immunopathology of multiple sclerosis: an overview. Brain Pathol 2007;17: 210–218.
18. Floyd RA, Zaleska MM, Harmon HJ. Possible involvement of iron and oxygen free radicals in aspects of agin in brain. In: Armstrong D, ed. Free radicals in molecular biology, aging, and disease. New York: Raven, 1984:143–161.
19. Levine SM, Chakrabarty A. The role of iron in the pathogenesis of experimental allergic encephalomyelitis and multiple sclerosis. Ann N Y Acad Sci 2004;1012:252–266.
20. Mehindate K, Sahlas DJ, Frankel D, et al. Proinflammatory cytokines promote glial heme oxygenase-1 expression and mitochondrial iron deposition: implications for multiple sclerosis. J Neurochem 2001;77:1386–1395.
21. Ruuls SR, Bauer J, Sontrop K, et al. Reactive oxygen species are involved in the pathogenesis of experimental allergic encephalomyelitis in Lewis rats. J Neuroimmunol 1995;56:207–217.
22. Gutteridge JM. Iron and oxygen radicals in brain. Ann Neurol 1992;32(suppl):S16–S21.
23. Drayer B, Burger P, Darwin R, et al. MRI of brain iron. AJR Am J Roentgenol 1986;147:103–110.
24. Bakshi R, Miletich RS, Kinkel PR, et al. High-resolution fluorodeoxyglucose positron emission tomography shows both global and regional cerebral hypometabolism in multiple sclerosis. J Neuroimaging 1998;8:228–234.
25. Ge Y, Jensen JH, Lu H, et al. Quantitative assessment of iron accumulation in the deep gray matter of multiple sclerosis by magnetic field correlation imaging. AJNR Am J Neuroradiol 2007;28:1639–1644.
26. Nordstrom DM, West SG, Andersen PA. Basal ganglia calcifications in central nervous system lupus erythematosus. Arthritis Rheum 1985;28:1412–1416.
27. Henry RG, Shieh M, Okuda DT, et al. Regional grey matter atrophy in clinically isolated syndromes at presentation. J Neurol Neurosurg Psychiatry 2008;79:1236–1244.
28. Adams CW. Perivascular iron deposition and other vascular damage in multiple sclerosis. J Neurol Neurosurg Psychiatry 1988;51:260–265.
29. LeVine SM, Torres MV. Morphological features of degenerating oligodendrocytes in twitcher mice. Brain Res 1992;587: 348–352.
30. Noseworthy JH, Lucchinetti C, Rodriguez M, Weinshenker BG. Multiple sclerosis. N Engl J Med 2000;343:938–952.
31. Prineas JW, Kwon EE, Cho ES, et al. Immunopathology of secondary-progressive multiple sclerosis. Ann Neurol 2001;50: 646–657.
32. Connor JR, Menzies SL, Burdo JR, Boyer PJ. Iron and iron management proteins in neurobiology. Pediatr Neurol 2001;25: 118–129.
33. Kidd D, Barkhof F, McConnell R, et al. Cortical lesions in multiple sclerosis. Brain 1999;122(pt 1):17–26.
34. Thompson AJ, Polman CH, Miller DH, et al. Primary progressive multiple sclerosis. Brain 1997;120(pt 6):1085–1096.
35. Hochmeister S, Grundtner R, Bauer J, et al. Dysferlin is a new marker for leaky brain blood vessels in multiple sclerosis. J Neuropathol Exp Neurol 2006;65:855–865.
36. Dousset V, Brochet B, Deloire MS, et al. MR imaging of relapsing multiple sclerosis patients using ultra-small-particle iron oxide and compared with gadolinium. AJNR Am J Neuroradiol 2006;27:1000–1005.
37. Vellinga MM, Oude Engberink RD, Seewann A, et al. Pluriformity of inflammation in multiple sclerosis shown by ultrasmall iron oxide particle enhancement. Brain 2008;131: 800–807.
38. Haacke EM, Xu Y, Cheng YC, Reichenbach JR. Susceptibility weighted imaging (SWI). Magn Reson Med 2004;52:612–618.
39. Kesselring J. [Prognosis in multiple sclerosis]. Schweiz Med Wochenschr 1997;127:500–505.
40. Tan IL, van Schijndel RA, Pouwels PJ, et al. MR venography of multiple sclerosis. AJNR Am J Neuroradiol 2000;21: 1039–1042.
41. Tallantyre EC, Brookes MJ, Dixon JE, et al. Demonstrating the perivascular distribution of MS lesions in vivo with 7-Tesla MRI. Neurology 2008;70:2076–2078.
42. Ge Y, Zohrabian VM, Grossman RI. Seven-Tesla magnetic resonance imaging: new vision of microvascular abnormalities in multiple sclerosis. Arch Neurol 2008;65:812–816.
43. Adams CW, Poston RN, Buk SJ. Pathology, histochemistry and immunocytochemistry of lesions in acute multiple sclerosis. J Neurol Sci 1989;92:291–306.
44. Ge Y, Law M, Johnson G, et al. Dynamic susceptibility contrast perfusion MR imaging of multiple sclerosis lesions: characterizing hemodynamic impairment and inflammatory activity. AJNR Am J Neuroradiol 2005;26:1539–1547.